B-splines Coupled with Quadrature Texture to Register Prostate Multimodal Images

Jhimli Mitra, Robert Marti, Arnau Oliver, Xavier Llado, Soumya Ghose, Joan C. Vilanova, Fabrice Mériaudeau

Noname manuscript No.
(will be inserted by the editor)

B-splines Coupled with Quadrature Texture to Register Prostate Multimodal Images

Jhimli Mitra · Robert Martí · Arnau Oliver · Xavier Lladó · Soumya Ghose · Joan C. Vilanova · Fabrice Meriaudeau

Received: date / Accepted: date

Abstract *Purpose:* Needle biopsy of the prostate is guided by Transrectal Ultrasound (TRUS) imaging. The TRUS images do not provide proper spatial localization of malignant tissues due to the poor sensitivity of TRUS to visualize early malignancy. Magnetic Resonance Imaging (MRI) has been shown to be sensitive for detection of early stage malignancy and therefore, a novel 2D deformable registration method that overlays pre-biopsy MRI onto TRUS images has been proposed.
Method: The registration method involves B-spline deformations with Normalized Mutual Information (NMI) as similarity measure computed from the texture images obtained from the amplitude responses of the directional quadrature filter pairs. Registration accuracy of the proposed method is evaluated by computing the Dice Similarity coefficient (DSC) and 95% Hausdorff Distance (HD) values for 20 patient datasets and Target Registration Error (TRE) for 18 patients only where homologous structures are visible in both the TRUS and transformed MR images.
Results: The proposed method and B-splines using NMI computed from intensities provide average TRE values of 2.64 ± 1.37 mm and 4.43 ± 2.77 mm respectively. Our method shows statistically significant improvement in TRE when compared to B-spline using NMI computed from intensities with Student's t-test $p = 0.02$. The proposed method shows 1.18 times improvement over Thin-plate splines registration with average TRE of 3.11 ± 2.18 mm. The mean DSC and the mean 95% HD values obtained with the proposed method of B-spline with NMI computed from texture are 0.943 ± 0.039 and 4.75 ± 2.40 mm respectively.
Conclusions: The texture energy computed from the quadrature filter pairs provides better registration accuracy for multimodal images than raw intensities. Low TRE values of the proposed registration method adds to the feasibility of it being used during TRUS guided biopsy.

Keywords Prostate multimodal registration · B-spline · quadrature filter · texture energy · normalized mutual information

J. Mitra*, R. Martí, A. Oliver, X. Lladó, S. Ghose
Universitat de Girona,Computer Vision and Robotics Group, Girona, Spain.
E-mail: jhimlimitra@yahoo.com, marly@eia.udg.edu, aoliver@eia.udg.edu, llado@eia.udg.edu, soumyaghose@gmail.com

J. C. Vilanova
Clínica Girona, Girona, Spain.
E-mail: kvilanova@comg.cat

F. Meriaudeau
*Université de Bourgogne, Le2i-UMR CNRS 5158, Le Creusot, France.
E-mail: fabrice.meriaudeau@u-bourgogne.fr

1 Introduction

Transrectal Ultrasound (TRUS) is routinely used for interventional needle biopsy of the prostate to detect prostate cancer. However, ultrasound images only provide very limited information about the location of prostate cancer. Cancer tissues are either hypoechoic or isoechoic in TRUS. The isoechoic cancer tissues account for about $24\% - 42\%$ [7]. As reported in [3] the probability to diagnose prostate cancer from TRUS biopsy alone is about $70\% - 80\%$. Therefore, the multicore biopsy technique used for needle biopsy oftens fails to extract positive samples and the number of rebiopsies thereby increases. It has been demonstrated in [36] that detection of prostate cancer using Magnetic Resonance Imaging (MRI) has a negative predictive value of 95%

or greater and also the accuracy of MRI to diagnose prostate cancer is 95%. Therefore, MRI may serve as a triage test for men deemed to be at risk of prostate cancer. In other words, if MRI has a negative predictive value $\geq 95\%$ for significant cancer then it might greatly reduce the number requiring biopsy, while at the same time increasing the yield of useful information for those who are sent for biopsy. Therefore, fusion of pre-biopsy MR images onto interventional TRUS images might increase the overall biopsy accuracy [22], [40], [34]. Fei et al. [12] registered interventional Magnetic Resonance Imaging (iMRI) slices to previously obtained high resolution MRI volume of prostate images for iMRI guided radio frequency thermal ablation of prostate cancer. A validation and integration for 3D TRUS guided robotic surgery for prostate brachytherapy was done by Wei et al. [38]. Hummel et al. [17] proposed a rigid registration for fusion of 2D intraoperative US with preoperative CT volume based on fiducials.

The prostate of the same patient may undergo deformations during the TRUS or MR imaging procedures due to full bladder or rectum, altered patient positions on the couch and inflation of the endorectal balloon inside the rectum containing the MR coil. Intended to cope with these deformations, nonrigid registration methods are applied for prostate multimodal fusion [28], [31], [5], [29], [8], [4]. Spline based deformations have been commonly used for prostate registration. Lu et al. [24] used Thin-plate Splines (TPS) warping to generate statistical volumetric model of prostate for localization of prostate cancer. However, the Target Registration Error (TRE) value of 295.66 pixels seemed to be too large to be used in clinical interventions. Prostate MR volumes were warped using TPS by Fei et al. [13] where the prostate centroid displacement was observed to be 0.6 mm. Vishwanath et al. [37] registered prostate histological slices and MR slices to detect prostate cancer using B-splines. Since the aim was to detect cancer, quantitative values related to registration accuracy were not presented. A recent work by Xiao et al. [39] proposed to build a spatial disease atlas of the prostate using both B-splines and TPS. However, only qualitative results were presented. Oguro et al. [30] registered pre- and intraoperative MR images for prostate brachytherapy. Dice Similarity Coefficient (DSC) value for the total gland was reported as 0.91 and the fiducial registration error was 2.3 ± 1.8 mm respectively. TRUS and MR multimodal registration for interventional biopsy was attempted by Mitra et al. [27]. The method was based on TPS with automatic point correspondences generated with an average DSC of 0.97 ± 0.01 for 4 patient datasets.

In this work a method to register TRUS and MR prostate 2D images with B-spline free-form deformations and quadrature filter pairs is presented. The B-spline registration uses uniform grids over the MR image and NMI is used as a similarity measure [32], [19]. However, the novelty of the proposal is to use directional quadrature filter pairs to transform both the MR and TRUS images into texture images obtained from the amplitude response of the filter pairs and use these transformed images for NMI computation. A similar method has been used by Jarc et al. [21] employing Law's texture to compute the MI in order to register far-infrared and visible spectrum gray-scale images. Francois et al. [15] used texture-based statistical measures to register carotid ultrasound volumes where the texture information was given by spatial Gabor filters. The remaining paper is organized with the details of the method in section 2. Results and discussions follow in section 3 with the conclusions in section 4.

2 Materials and Methods

2.1 The Proposed Method and Algorithm

The proposed method uses B-spline deformations to register 2D MR slice corresponding to the 2D TRUS slice. This work is a feasibility study (improving on registration accuracy) on the type deformable registration algorithm that may be used during prostate biopsy for accurate extraction of biopsy samples. Therefore, the corresponding 2D axial MR slice of the respective axial TRUS slice is identified by an expert that closely match each other. In the clinical context, the idea would be to track the z-coordinate of the TRUS axial 2D slice with an electromagnetic tracking device attached to the TRUS probe during biopsy and find an automatic slice correspondence with a reconstructed 3D TRUS volume and finally register to the 3D MR volume [40]. In our work, once the slice correspondences are established, the prostate in each of the images is then manually segmented. However, we plan to use some automatic segmentation methods proposed by Shen et al. [33], Cosio [9] and Ghose et al. [16] for automatic real-time fusion of multimodal prostate images. The optimal B-spline deformations are obtained by maximizing the NMI as similarity measure. The NMI of the fixed TRUS and the moving MR images is computed from the image texture energies obtained from the amplitude response of the directional quadrature filters (section 2.3). The advantage of computing NMI by this method is that the gray level differences in the TRUS and MR modalities are minimized, enhancing the inherent texture information

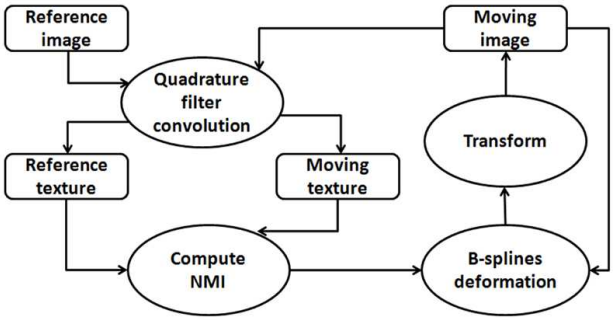

Fig. 1 A schematic diagram of the proposed algorithm.

of the prostate. A schematic diagram in Fig. 1 shows the work flow of the proposed algorithm.

2.2 Registration using B-splines

A common technique to represent a free-form deformation is to employ spline functions as B-splines [32]. B-splines consist of a set of control points that can be locally controlled on the image domain. Although, the original B-splines equation is formulated for 3D-deformable objects [32], [19], the spline functions in this paper are represented for 2D images.

Let $\Omega = \{(x,y)|0 \leq x < X, 0 \leq y < Y\}$ represent the image domain. The transformation between the moving and fixed images is given by $\mathbf{T}$**:**$(x,y) \mapsto (x',y')$, where any point (x,y) of the moving image is mapped onto its corresponding point (x',y') on the fixed image. Given a mesh of control points on the moving image with a control point defined as $\phi_{i,j}$ with uniform spacing of δ mm, the nonrigid transformation $\mathbf{T}$ is defined by B-spline functions as

$$\mathbf{T}(x,y) = \sum_{l=0}^{3}\sum_{m=0}^{3} B_l(u)B_m(v)\phi_{i+l,j+m} \tag{1}$$

where $i = \lfloor x/\delta \rfloor - 1$, $j = \lfloor y/\delta \rfloor - 1$, $u = x/\delta - \lfloor x/\delta \rfloor$ and $v = y/\delta - \lfloor y/\delta \rfloor$. $\lfloor . \rfloor$ is the floor function and B_l represents the l^{th} basis function of the cubic B-spline functions such that

$$\begin{aligned} B_0(u) &= (1-u^3)/6 \\ B_1(u) &= (3u^3 - 6u^2 + 4)/6 \\ B_2(u) &= (-3u^3 + 3u^2 + 3u + 1)/6 \\ B_3(u) &= u^3/6. \end{aligned} \tag{2}$$

The B-spline free-form deformations are locally controlled because the deformation at any point (x,y) is controlled by its neighboring 4×4 control points. B-splines provide a wide range of deformations by organizing the mesh of control points and the images in a hierarchy [14], i.e. the distance between the control points decrease introducing more control points while the images move from coarser to finer levels using a multiresolution Gaussian pyramid. The B-spline control points grid refinement is done using the standard splitting matrix [41].

The similarity measure used for B-splines deformation is NMI (described in details in section 2.4) between the moving (M) and the fixed (F) images and the optimization is solved using a quasi-Newton optimization method as "Limited Memory Broyden-Fletcher-Glodfarb-Shanno" (L-BFGS) algorithm [23].

2.3 Quadrature Filters

Band-pass quadrature filters have been used in computer vision to access multi-scale image information like local-phase, energy, angular frequency etc. Central to the theory of quadrature filters in the analytical domain is the Hilbert transform [6]. The analytical signal of a 1D real signal $f(x)$ is given by

$$f_A(x) = f(x) - if_{\mathcal{H}}(x); \tag{3}$$

where $i = \sqrt{-1}$ and $f_{\mathcal{H}}(x)$ is the Hilbert transform of $f(x)$ defined by:

$$\begin{aligned} f_{\mathcal{H}}(x) &= \frac{1}{\pi}\int_{-\infty}^{+\infty} \frac{f(\tau)}{\tau - x} d\tau \\ \Leftrightarrow F_{\mathcal{H}}(\omega) &= F(\omega).i\ \mathrm{sign}(\omega), \end{aligned} \tag{4}$$

where, $F(\omega)$ is the Fourier transform of $f(x)$ and

$$\mathrm{sign}(\omega) = \begin{cases} -1 & \omega < 0 \\ +1 & \omega \geq 0 \end{cases} \tag{5}$$

Therefore, the analytical signal in Fourier domain is obtained from (3) and (5) as

$$F_A(\omega) = F(\omega).\left[1 + \mathrm{sign}(\omega)\right]. \tag{6}$$

To compute the local features of an image, localization of both space and frequency is required and is not possible directly from the resulting analytical signal since the Hilbert transform or analytical signal in (3) and (5) is defined over the entire signal. Therefore, an alternative approach is to compute the local phase or energy from the filtered version of the signal. The filter is an even, symmetric, zero-DC filter $f_e(x)$ and its odd counterpart is $f_o(x)$ which is the Hilbert transform of $f_e(x)$, hence they are in quadrature. Therefore, the analytical signal can be written as

$$\begin{aligned} \hat{f}_A(x) &= f_e(x) * f(x) - i\mathcal{H}(f_e(x) * f(x)) \\ &= (f_e(x) - i\mathcal{H}(f_e(x)) * f(x) \\ &= (f_e(x) - if_o(x)) * f(x). \end{aligned} \tag{7}$$

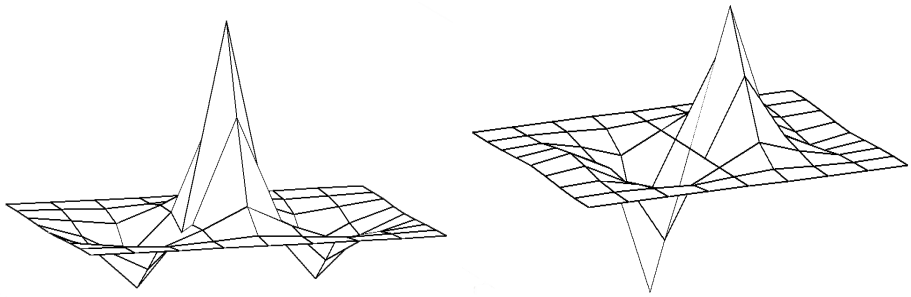

Fig. 2 Even and Odd log-Gabor quadrature filter pairs in spatial domain.

Where $\mathcal{H}(.)$ is the Hilbert transform and '*' is the 1-D convolution operator.

In practice, an approximation of the local amplitude or energy ($\hat{A}(x)$) and phase ($\hat{\phi}(x)$) is obtained by using band-pass quadrature even and odd filter pair, $f_e(x)$ and $f_o(x)$ respectively, where,

$$\hat{A}(x) = \sqrt{[f_e(x) * f(x)]^2 + [f_o(x) * f(x)]^2} \tag{8}$$

$$\hat{\phi}(x) = \arctan\{f_e(x) * f(x)/f_o(x) * f(x)\}. \tag{9}$$

A generalization of quadrature filters in 2-D is provided as a set of filters tuned to a particular orientation and are therefore called directional quadrature filters [20].

The magnitude of the complex filter response with images gives the power portions of the texture process contained in different spectral bands [1]. Log-Gabor quadrature filters are used in this paper that are Gaussian functions on logarithmic scale. The 1-D representation of log-Gabor function in frequency domain is given by

$$G_l(\omega) = \exp\left(-\frac{\ln^2(\omega/\omega_0)}{2\ln^2(\kappa_\beta)}\right) \tag{10}$$

where ω_0 is the peak tuning frequency at $\pi/3$ and $0 < \kappa_\beta < 1$.

$$\kappa_\beta = \exp\left(-\frac{1}{4}\sqrt{2\ln(2)}\beta\right),$$

where β is the bandwidth fixed to 2 octaves. The peak tuning frequency and bandwidth are optimized values obtained from the MATLAB toolbox provided by Andersson and Knutsson [2]. Quadrature filters in directions $0°, 45°, 90°$ and $135°$ are used and the individual even and odd filter responses are added to provide the magnitude of the combined filter response. The even and odd filters tuned to $0°$ are shown in Fig. 2. Fig. 3 shows the texture energies of the fixed TRUS and the moving MR images when the 4 directional even-odd quadrature filter pairs are applied. It is evident that the gray level differences between the internal structures of the prostate are minimized in MR image as well as the shadow regions have disappeared in the TRUS image.

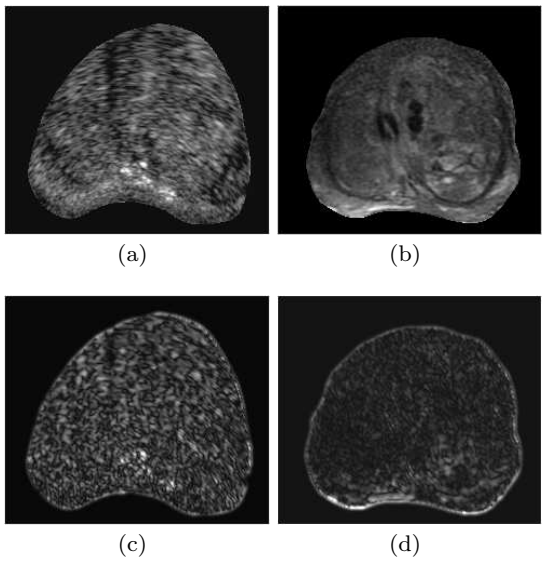

Fig. 3 Application of quadrature filters on TRUS and MR images. (a) and (c) are the fixed TRUS image and its corresponding quadrature texture; and (b) and (d) are the moving MR image and its corresponding quadrature texture respectively.

2.4 Normalized Mutual Information

The magnitude responses of the quadrature filters obtained in section 2.3 are used to compute the NMI between the moving and fixed images. The NMI is an information theoretic measure that tries to reduce the joint entropy of the images [35] and is given by

$$\text{NMI} = \zeta_{similarity} = \frac{H(M) + H(F)}{H(M,F)} \tag{11}$$

where $\zeta_{similarity}$ is the similarity measure for B-splines registration that is maximized in the process, $H(M)$ and $H(F)$ are the marginal entropies of the moving (M) and fixed (F) images respectively, and $H(M,F)$ is the joint entropy of the images. $H(M,F)$ can be written using probability theory as

$$H(M,F) = -\sum_{m,f} p(m,f)\log[p(m,f)], \tag{12}$$

where, $p(m, f)$ is the joint probability distribution of the images obtained from their joint histogram.

2.5 Data and Analysis

The proposed method is evaluated with datasets of 20 patients with average prostate volume of 56.7 ± 22.0 cm^3. The TRUS images were acquired with 6.5MHz side-firing probe with SIEMENS Allegra and TOSHIBA Xario machines and the axial T2 fast relaxation fast spin echo MRI slices with slice thickness of 3 mm, repetition time of $3460 - 3860$ millisecs and echo time of $113.62 - 115.99$ millisecs were acquired with GE Signa HDxt. The axial middle slices in TRUS are chosen for which the corresponding axial MR slices are identified by an expert. Ideally the axial MR slice corresponding and parallel to the axial TRUS slice should be obtained by rotating the MR volume in accordance with the rotational angle of the TRUS slice and then resampling the axial MR slice parallel to the axial TRUS slice under observation. However, we have not quantified the TRUS rotational angle in our current experimental process. The prostate is manually segmented from both the moving MR and fixed TRUS images. A NMI-based affine transformation between the TRUS and the MR images is followed by the free-form B-spline deformation. An uniform initial B-spline control grid with a spacing of 64×64 is placed on the moving image with an average image size of 256×256. Fig. 4 shows the uniform B-spline control grids on the moving MR image of size 219×249 at the initial and final resolutions. The B-splines deform at each resolution to maximize the NMI computed from texture images that are obtained from the magnitudes of quadrature filter responses.

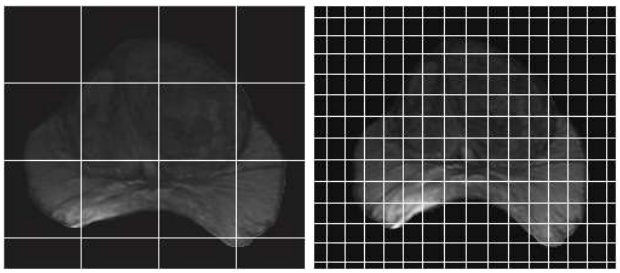

(a) (b)

Fig. 4 B-splines control grid with 2 refinements over the initial placement on the moving MR image of size 219×249. (a) shows the initial placement of the B-spline grids with 64×64 pixel spacing on the moving MR image and (b) shows the final set of B-spline control grids on the transformed moving image.

Common metrics to evaluate registration accuracies are DSC [10], TRE [26], [25] and 95% Hausdorff Distance (HD) [18]. DSC is a measure of overlap of the same labels (E) between the transformed moving image ($M(E)$) and the fixed image ($F(E)$) and is given by

$$\mathrm{DSC} = \frac{2(M(E) \cap F(E))}{M(E) + F(E)}. \tag{13}$$

A target is an anatomical landmark in the patient's body and is normally the centroid of a lesion, tumor, gland, etc. that is not used to compute the transformation of the moving image to the fixed image. TRE is the root mean square distance of such homologous targets tp_i and tq_i, $i = 1, 2, \cdots, N$ on the moving and the fixed images respectively and is given by

$$\mathrm{TRE} = \frac{1}{N}\sqrt{\sum_{i=1}^{N} (\mathbf{T}(tp_i) - tq_i)^2} \tag{14}$$

where, $\mathbf{T}(.)$ is the transformation of the moving image. The targets used in our experiments are primarily centroids of lesions and tumors in central gland, prostatic urethra, sometimes centroids of tumor in peripheral region and the centroid of the central gland in few cases where lesions or other homologous structures are not visible in TRUS as in the corresponding MRI. The repeatability error in the localization of the targets is given as the Target Localization Error (TLE) computed from the centroids of manually selected regions from 5 independent trials by an experienced radiologist.

Given a set of finite points $A = \{a_1, \ldots, a_p\}$ and $B = \{b_1, \ldots, b_q\}$, the Hausdorff distance between the point sets is defined by

$$HD(A, B) = \max(h(A, B), h(B, A)) \tag{15}$$

where

$$h(A, B) = \max_{a \in A}(\min_{b \in B} \|a - b\|) \tag{16}$$

and $\|.\|$ is the Euclidean norm.

We have compared the proposed method against two spline-based registration methods; 1) B-splines registration that maximizes the NMI computed from the raw intensities of the multimodal images [32], and 2) registration using TPS that uses contour-based automatic correspondences to solve the affine and TPS weight parameters [27].

Table 1 A comparison of registration accuracies of the B-spline registration with NMI computed from intensities, from texture and TPS registration. μ is the mean and σ is the standard deviation of the measures.

Patient#	**B-spline Registration**								**TPS Registration**			
	NMI from Intensities Rueckert et al. [32]				***NMI from Texture***				Mitra et al. [27]			
	DSC	TRE (mm)	TLE (mm)	HD (mm)	DSC	TRE (mm)	TLE (mm)	HD (mm)	DSC	TRE (mm)	TLE (mm)	HD (mm)
1	0.902	5.07	0.10	9.35	0.896	4.09	0.22	7.31	0.971	9.36	0.22	1.84
2	0.980	0.37	0.09	1.07	0.964	1.50	0.14	1.30	0.957	3.98	0.10	2.32
3	0.973	-	-	2.08	0.953	-	-	5.45	0.974	-	-	2.09
4	0.985	1.91	0.28	1.07	0.962	1.40	0.29	3.96	0.982	5.21	0.49	1.40
5	0.889	9.08	0.04	8.06	0.869	5.65	0.05	6.76	0.972	2.11	0.07	2.35
6	0.869	6.11	0.04	6.16	0.975	2.70	0.07	2.23	0.979	1.17	0.05	2.32
7	0.959	0.90	0.12	5.04	0.889	1.94	0.09	8.82	0.977	4.43	0.12	2.61
8	0.976	4.70	0.03	3.38	0.964	1.11	0.10	5.81	0.978	3.57	0.05	2.96
9	0.960	-	-	4.93	0.982	-	-	1.32	0.978	-	-	2.39
10	0.952	8.29	0.09	5.98	0.981	4.04	0.13	1.04	0.972	6.09	0.04	1.98
11	0.962	6.12	0.04	3.03	0.950	1.69	0.04	3.72	0.972	2.98	0.12	2.22
12	0.944	1.58	0.25	4.60	0.934	0.31	0.16	5.18	0.971	2.44	0.12	5.00
13	0.961	1.00	0.05	4.83	0.878	3.42	0.05	7.39	0.980	3.06	0.07	1.84
14	0.896	7.32	0.05	6.50	0.965	1.85	0.05	3.12	0.986	1.75	0.07	0.82
15	0.942	5.01	0.05	6.06	0.948	2.32	0.13	5.02	0.968	2.29	0.07	2.22
16	0.974	7.27	0.13	2.90	0.950	4.71	0.13	6.50	0.970	1.86	0.07	2.71
17	0.894	4.32	0.12	7.18	0.872	3.22	0.23	7.64	0.982	0.18	0.32	1.04
18	0.985	0.51	0.26	2.32	0.975	1.77	0.29	2.87	0.982	0.91	0.26	1.64
19	0.936	5.12	0.19	7.01	0.969	2.91	0.43	7.09	0.983	1.47	0.23	1.66
20	0.939	5.03	0.20	5.51	0.975	2.83	0.21	2.45	0.973	3.11	0.30	2.08
μ	**0.944**	**4.43**	**0.12**	**4.85**	**0.943**	**2.64**	**0.16**	**4.75**	**0.975**	**3.11**	**0.15**	**2.17**
σ	**0.036**	**2.77**	**0.08**	**2.30**	**0.039**	**1.37**	**0.11**	**2.40**	**0.007**	**2.18**	**0.12**	**0.85**

3 Results and Discussions

The registration accuracies of our method are evaluated in terms of DSC and 95% HD values for 20 patients and TRE and TLE values for 18 patients i.e. only where homologous structures are visible both in TRUS and the transformed MR images. Table 1 shows the DSC, TRE, TLE and 95% HD values as obtained from the experiments for B-spline deformations with NMI computed from intensities [32], our method for B-spline deformations with NMI computed from textures and TPS registration [27]. A statistically significant reduction with two-tailed t-test $p = 0.02$ is observed in the average TRE value for B-splines with NMI computed from texture when compared to B-splines with NMI computed from intensities with 2.64 ± 1.37 mm and 4.43 ± 2.77 mm respectively. Our proposed method shows an improvement of 1.18 times in TRE when compared with TPS registration with average TRE of 3.11 ± 2.18 mm. However, this improvement of average TRE over TPS is not statistically significant. The average TLE for all the methods are similar with 0.16 ± 0.11 mm, 0.12 ± 0.08 mm and 0.15 ± 0.12 mm for our method, B-splines with NMI from intensities and TPS registration respectively. It is observed from Table 1 that TLE is normally higher for patient cases where the centroid of a larger region is considered as the target.

The DSC value is a global measure of region overlap and the average DSC values for our method of B-splines with NMI computed from texture, B-splines with NMI computed from intensities and TPS registration are 0.943 ± 0.039, 0.944 ± 0.036 and 0.975 ± 0.007 respectively. 95% HD provides the contour accuracy for which the average values of 4.75 ± 3.40 mm, 4.85 ± 2.30 mm and 2.17 ± 0.85 mm are obtained for our method of B-splines with NMI from texture, B-splines with NMI from intensties and TPS respectively. We observe that TPS registration based on control points placed over the contours always has higher average DSC and lower average HD values over the proposed B-splines registration with statistical significance (two-tailed t-test) of $p < 0.001$ and $p < 0.0001$ for DSC and 95% HD measures respectively.

TRE values of all patients are much lower with the proposed method when compared to the B-spline method with NMI computed from intensities except for patients 2, 7, 13 and 18 where the dark shadows near the edges of the TRUS images are misinterpreted as the black background. Higher DSC values are obtained from the proposed method when compared to B-spline with NMI

computed from intensities especially for patients 6, 9, 10, 14, 15, 19 and 20 and for patients 2, 9, 10 and 20 when compared to TPS.

Fig. 5 shows the qualitative B-spline registration using NMI from raw intensities, using NMI from texture and the TPS registration in the form of checkerboards for 6 patients (patient 6, 8, 10, 11, 13 and 15). As seen in Fig. 5 for patients 6 (column 1), 10 (column 3) and 15 (column 6), the checkerboards (row 6) show good region overlaps that are also evident from Table 1 for the proposed method. TRE is a reliable measure of registration accuracy than region overlap measure specially when localization of biopsy site is involved. Therefore, in spite of the less satisfactory region overlaps in Fig. 5 for the proposed method (row 6) with patients 8 (column 2), 11 (column 4) and 15 (column 6) when compared to other methods (rows 4 and 8), lower TRE values are obtained for the same patient cases with our proposed method as seen in Table 1. In Fig. 5 we observe poor region overlaps for patients 11 and 13 in columns 4 and 5 respectively. There may be two reasons for the poor registration accuracy around the prostate contour, 1) acoustic shadows in TRUS images around the rectum do not provide any texture information and are considered homogeneous with the black background, and 2) part of the contour of the moving image may lie far from the respective fixed image contour. In both these cases, the control grids placed on the moving image around the contour consider a large part of the black background for the maximization of NMI with the corresponding TRUS (textured) region and therefore the maximization process fails to reach a global maximum. However, blurring of the prostate around the bladder or rectum would not affect the contour registration accuracy since blurred regions still may contain some texture. As seen for patient 15 (row 1, column 6) that the blurring of the prostate around the rectum in TRUS does not affect the overlap accuracy. It is also observed that shadow artifacts and calcifications inside the prostate do not affect the contour registration accuracy. For instance, for patient 11 (row 1, column 4), the acoustic shadow region inside the prostate does not affect the overlap accuracy; however, the large part of the shadow on the lower-right contour region deteriorates the contour overlap accuracy.

The texture obtained from the magnitude of directional quadrature filter transforms of an image measures the power portions of the image. The MR and TRUS images have varied gray-level intensities and contrasts. Therefore, transforming the MR and TRUS images as texture energy images homogenizes the intensity variations between them and reveals the underlying prostate architectural information that is common to both the modalities. Hence, the proposed method shows better registration accuracies in terms of TRE than traditional B-splines deformation with NMI from intensities. The proposed algorithm is validated only on TRUS-MR slices from the prostate mid-gland region and the performance of the same on the base and apex regions is yet to be validated.

The algorithms are implemented in MATLAB 2009b with a machine configuration of 1.66 MHz Core2Duo processor and 2 GB memory. The average time requirements of our method of B-splines with NMI computed from texture, B-splines with NMI computed from intensities and TPS registrations are 797.72 ± 202.59 secs, 147.25 ± 43.81 secs and 76.22 ± 29.79 secs respectively. The computation time includes the time for affine and nonrigid registrations for each of the methods. The obvious reason of B-splines with NMI computed from texture being computationally expensive is due to the use of 4 quadrature convolutions for each of the fixed and moving images at each resolution of B-splines deformations. The lowest time of 397 secs and the maximum time 1316 secs are recorded for the proposed method. However, quadrature convolution and registration of $256 \times 256 \times 256$ 3D volumes are achievable at 3.05 secs when programmed in GPU [11]. Therefore, parallelization of the convolutions and our algorithm implemented on GPU would ideally reduce the execution time to less than 3 secs which is closer to the clinical requirement.

4 Conclusions

A method to register TRUS and MR prostate 2D images have been presented that uses B-spline deformations with a novel method of computing the NMI. The NMI as similarity measure for the registration is computed from texture energy of the images obtained from magnitude of the directional quadrature filter pair responses. Log-Gabor filters with narrow bandwidth has been used that allows to measure power portions of the signal representing texture energy in case of 2D TRUS and MR images. NMI computation involves reduction of entropy of the images. The entropy between TRUS and MR raw intensity images is typically more than the entropy of texture images due to variations in the gray-levels. Therefore, B-spline registration with NMI computed from texture images provides more average accuracy in terms of TRE than that with NMI computed from intensity images. We observed from the experiments that the average DSC and 95% HD values for TPS registration show smaller error compared to the proposed method and B-splines with NMI computed from intensities. This is due to the fact that the TPS registration in [27] is based on control points primarily

placed on prostate contour. This results in higher contour accuracy (related to both DSC and HD measures), while B-spline control points are uniformly spread over the prostate image. Since the final aim is accurate localization of biopsy samples and TRE provides a measure of registration accuracy for localized regions, it may be better to choose TRE over DSC or other contour accuracy measures. In this respect our method of B-splines with NMI computed from texture shows statistically significant improvement over B-splines with NMI computed from intensitites; and 1.18 times improvement over TPS registration. However, if the clinical requirement is contour accuracy, TPS registration may be preferred over the B-splines registration.

The proposed method may be extended to 2D-3D registration with the help of an electromagnetic tracking device eliminating the issue of choosing the slice correspondence by an expert. Considering the feasibility of the method of being used for clinical interventions, the entire process may be automated and the algorithm can be implemented on a GPU to be used during real-time interventional needle biopsy procedures.

ACKNOWLEDGMENTS

This research is a part of the PROSCAN project of the VICOROB laboratory of University of Girona, Catalunya, Spain. The authors would like to thank VALTEC 08-1-0039 of Generalitat de Catalunya, Spain and Conseil Régional de Bourgogne, France for funding this research.

References

1. Aach, T., Kaup, A., Mester, R.: On texture analysis: Local energy transforms versus quadrature filters. Signal Processing **45**, 173–181 (1995)
2. Andersson, M., Knutsson, H.: Adaptive filtering. http://www.imt.liu.se/edu/courses/TBMI02 (2010)
3. Arcangeli, C.G., Ornstein, D.K., Keetch, D.W., Andriole, G.L.: Prostate-specific antigen as a screening test for prostate cancer-The United States experience. The Urologic Clinics of North America **24**(2), 299–306 (1997)
4. Baumann, M., Mozer, P., Daanen, V., Troccaz, J.: Prostate biopsy assistance system with gland deformation estimation for enhanced precision. MICCAI, LNCS **5761**, 57–64 (2009)
5. du Bois d'Aische, A., Craene, M.D., Haker, S., Weisenfeld, N., Tempany, C., Macq, B., Warfield, S.K.: Improved non-rigid registration of prostate MRI. MICCAI, LNCS **3216**, 845–852 (2005)
6. Boukerroui, D., Noble, J.A., Brady, M.: On the choice of band-pass quadrature filters. Journal of Mathematical Imaging and Vision **21**, 53–80 (2004)
7. Carroll, P., Shinohara, K.: Transrectal ultrasound guided prostate biopsy. Tech. rep., Department of Urology, University of California, San Francisco (2010). Http://urology.ucsf.edu/patientGuides.html, accessed [30th Dec, 2010].
8. Chen, T., Kim, S., Zhou, J., Metaxas, D., Rajagopal, G., Yue, N.: 3D meshless prostate segmentation and registration in image guided radiotherapy. MICCAI, LNCS **5761**, 43–50 (2009)
9. Cosío, F.A.: Automatic initialization of an Active Shape Model of the prostate. Medical Image Analysis **12**, 469–483 (2008)
10. Dice, L.R.: Measures of the amount of ecologic association between species. Ecology **26**(3), 297–302 (1945)
11. Eklund, A., Andersson, M., Knutsson, H.: Phase based volume registration using CUDA. IEEE ICASSP pp. 658–661 (2010)
12. Fei, B.W., Duerk, J.L., Boll, D.T., Lewin, J.S., Wilson, D.L.: Slice-to-volume registration and its potential application to interventional MRI-guided radio-frequency thermal ablation of prostate cancer. IEEE Transactions on Medical Imaging **22**(4), 515–525 (2003)
13. Fei, B.W., Kemper, C., Wilson, D.L.: A comparative study of warping and rigid body registration for the prostate and pelvic MR volumes. Computerized Medical Imaging and Graphics **27**, 267–281 (2003)
14. Forsey, D.R., Barrels, R.H.: Hierarchcal B-spline refinement. Computer Graphics **22**(4), 205–212 (1988)
15. Francois, R., Fablet, R., Barillot, C.: Robust statistical registration of 3D ultrasound images using texture information. ICIP **1**, I–581–4 (2003)
16. Ghose, S., Oliver, A., Martí, R., Lladó, X., Freixenet, J., Vilanova, J., Meriaudeau, F.: Texture guided Active Appearance Model propagation for prostate segmentation. MICCAI Workshop on Prostate Cancer Imaging, Computer Aided Diagnosis, Prognosis and Intervention **LNCS 6367**, 111–120 (2010)
17. Hummel, J., Figl, M., Bax, M., Bergmann, H., Birkfellner, W.: 2D/3D registration of endoscopic ultrasound to CT volume data. Physics in Medicine and Biology **53**, 4303–4316 (2008)
18. Huttenlocher, D.P., Klanderman, G.A., Rucklidge, W.J.: Comparing images using the Hausdorff distance. IEEE Transaction in Pattern Analysis and Machine Intelligence **15**(9), 850–863 (1993)
19. Ino, F., Ooyama, K., Hagihara, K.: A data distributed parallel algorithm for nonrigid image registration. Parallel Computing **31**, 19–43 (2005)
20. Jähne, B.: Digital Image Processing, 6th edn. Springer-Verlag (2005)
21. Jarc, A., Perš, J., Rogelj, P., Perše, M., Kovačič, S.: Texture features for affine registration of thermal (FLIR) and visible images. Computer Vision Winter Workshop 2007 (2007)
22. Kaplan, I., Oldenburg, N.E., Meskell, P., Blake, M., Church, P., Holupka, E.J.: Real time MRI-ultrasound image guided stereotactic prostate biopsy. Magnetic Resonance Imaging **20**, 295–299 (2002)
23. Liu, D.C., Nocedal, J.: On the limited memory method for large scale optimization. Mathematical Programming B **45**(3), 503–528 (1989)
24. Lu, J., Srikanchana, R., McClain, M., Wang, Y., Xuan, J., Sesterhenn, I.A., Freedman, M.T., Mun, S.K.: A statistical volumetric model for characterization and visualization of prostate cancer. Proc. of SPIE **3976**, 142–153 (2000)
25. Maurer, C.R., Fitzpatrick, J.M., Wang, M.Y., Member, S., Galloway, R.L., Maciunas, R.J., Allen, G.S.: Registration of head volume images using implantable fidu-

cial markers. IEEE Transactions on Medical Imaging **16**, 447–462 (1997)
26. Maurer, C.R., McCrory, J.J., Fitzpatrick, J.M.: Estimation of accuracy in localizing externally attached markers in multimodal volume head images. Proceedings of SPIE Medical Imaging **1898**, 43–54 (1993)
27. Mitra, J., Oliver, A., Martí, R., Lladó, X., Vilanova, J.C., Meriaudeau, F.: A thin-plate spline based multimodal prostate registration with optimal correspondences. SITIS'10 pp. 7–11 (2010)
28. Mizowaki, T., Cohen, G.N., Fung, A.Y.C., Zaider, M.: Towards integrating functional imaging in the treatment of prostate cancer with radiation: The registration of the MR spectroscopy imaging to ultrasound/CT images and its implementation in treatment planning. Intl. Journal of Radiation Oncology Biol. Phys. **54**(5), 1558–1564 (2002)
29. Narayanan, R., Kurhanewicz, J., Shinohara, K., Crawford, E.D., Simoneau, A., Suri, J.S.: MRI-ultrasound registration for targeted prostate biopsy. IEEE ISBI 2009 pp. 991–994 (2009)
30. Oguro, S., Tokuda, J., Elhawary, H., Haker, S., Kikinis, R., Tempany, C.M., Hata, N.: MRI signal intensity based B-spline nonrigid registration for pre- and intraoperative imaging during prostate brachytherapy. Magnetic Resonance Imaging **30**(5), 1052–1058 (2009)
31. Reynier, C., Troccaz, J., Fourneret, P., Dusserre, A., Gay-Jeune, C., Descotes, J.L., Bolla, M., Giraud, J.Y.: MRI/TRUS data fusion for prostate brachytherapy. preliminary results. Medical Physics **31**(6), 1568–1575 (2004)
32. Rueckert, D., Sonoda, L.I., Hayes, C., Hill, D.L.G., Leach, M.O., Hawkes, D.J.: Nonrigid registration using free-form deformations: Application to breast MR images. IEEE Transactions on Medical Imaging **18**(8), 712–721 (1999)
33. Shen, D., Zhan, Y., Davatzikos, C.: Segmentation of prostate boundaries from ultrasound images using statistical shape model. IEEE Transactions on Medical Imaging **22**, 539–551 (2003)
34. Singh, A.K., Kruecker, J., Xu, S., Glossop, N., Guion, P., Ullman, K., Choyke, P.L., Wood, B.J.: Initial clinical experience with real-time transrectal ultrasonography-magnetic resonance imaging fusion-guided prostate biopsy. British Journal of Urology International **101**(7), 841–845 (2008)
35. Studholme, C., Hill, D.L.G., Hawkes, D.J.: An overlap invariant entropy measure of 3D medical image alignment. Pattern Recognition **72**(1), 71–86 (1999)
36. Vilanova, J.C.: Usefulness of prebiopsy multi-functional and morphologic MRI combined with the free-to-total PSA ratio in the detection of prostate cancer. AJR (In press)
37. Vishwanath, S., Bloch, B.N., Rosen, M., Chappelow, J., Toth, R., Rofsky, N., Lenkinski, R., Genega, E., Kalyanpur, A., Madabhushi, A.: Integrating structural and functional imaging for computer assisted detection of prostate cancer on multi-protocol *In Vivo* 3 Tesla MRI. Proceedings of SPIE **7260**, 72,603I.1–12 (2009)
38. Wei, Z., Wan, G., Gardi, L., Mills, G., Downey, D., Fenster, A.: Robot-assisted 3D-TRUS guided prostate brachytherapy: System integration and validation. Medical Physics **31**(3), 539–548 (2004)
39. Xiao, G., Bloch, B., Chappelow, J., Genega, E., Rofsky, N., Lenkinski, R., Madabhushi, A.: A structural-functional MRI-based disease atlas:application to computer-aided-diagnosis of prostate cancer. Proc. of SPIE **7623**, 762,303.1–12 (2010)
40. Xu, S., Kruecker, J., Turkbey, B., Glossop, N., Singh, A.K., Choyke, P., Pinto, P., Wood, B.J.: Real-time MRI-TRUS fusion for guidance of targeted prostate biopsies. Computer Aided Surgery **13**(5), 255–264 (2008)
41. Yamaguchi, F.: Curves and Surfaces in Computer Aided Geometric Design. Springer (1988)

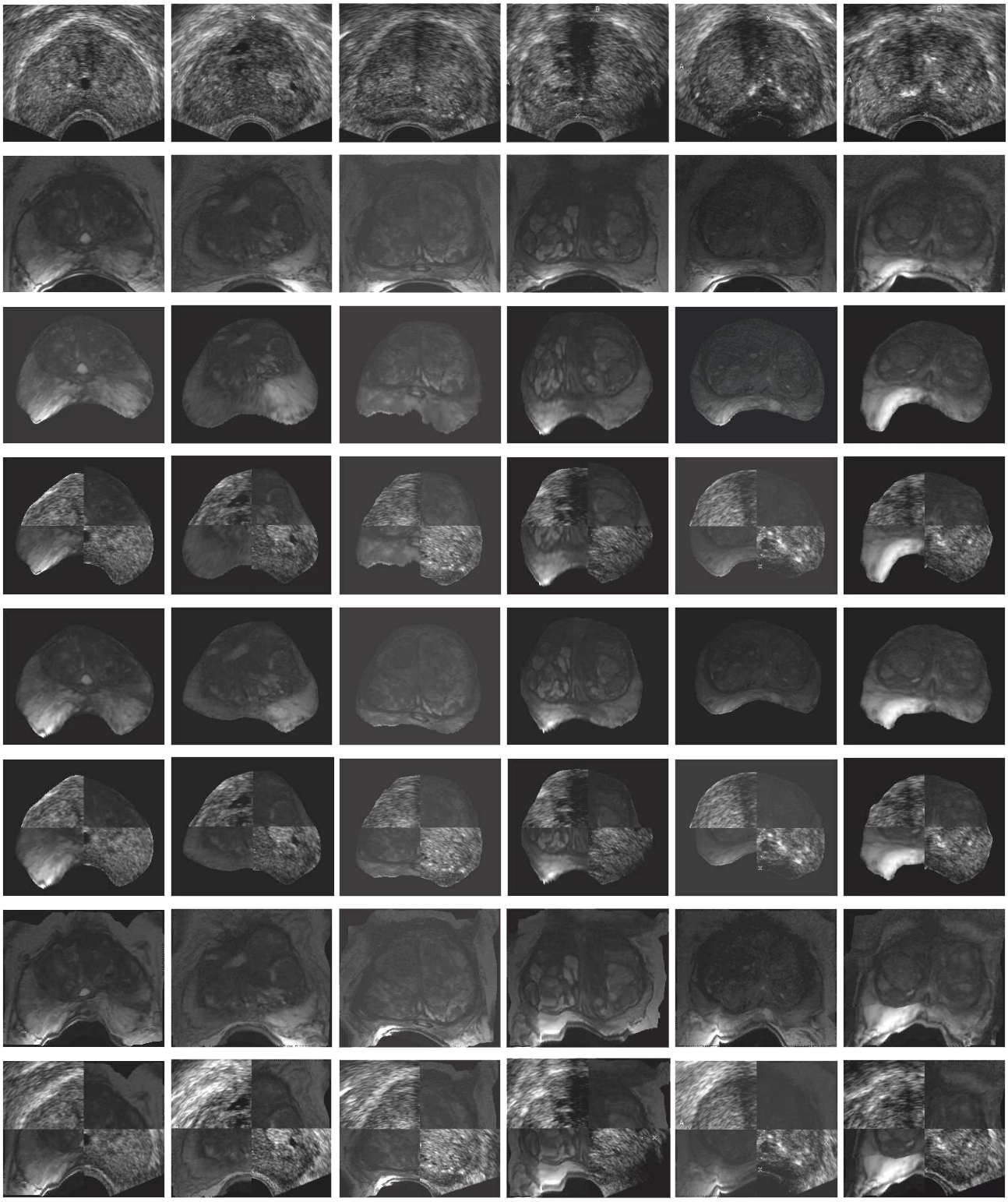

Fig. 5 Qualitative B-spline registration using NMI from intensity images, NMI from texture images and TPS registration. Patients 6, 8, 10, 11, 13 and 15 in columns. 1^{st} row shows the fixed TRUS slices, 2^{nd} row shows the moving MR slices, $3^{rd} - 4^{th}$ rows show the fused MR and the checkerboards for B-spline using NMI from intensity images, $5^{th} - 6^{th}$ rows show the fused MR and the checkerboards for B-spline using NMI from texture images and $7^{th} - 8^{th}$ rows show the fused MR and checkerboard for TPS registration.